Mean Flow Generation on a Continental Margin by Periodic Wind Forcing

D. W. DENBO AND J. S. ALLEN

School of Oceanography, Oregon State University, Corvallis 97331

(Manuscript received 12 April 1982, in final form 26 August 1982)

ABSTRACT

The generation of an alongshore mean flow by the nonlinear interaction of forced barotropic shelf waves over a continental margin is studied using a wind-forced, f-plane model with bottom friction in an attempt to develop a model for poleward eastern boundary undercurrents. It is assumed that the Rossby number is small and that the flow obeys a long-wave approximation. A periodic alongshore wind stress traveling along the coast forces the fluid by a nonzero wind stress at the coast (coastal forcing) or by a wind-stress-curl-driven oceanic flow that impinges on the slope (interior forcing). Expressions are derived for the alongshore (v) and cross-shelf (u) mean velocities in terms of the lowest order periodic velocities. An expression for the correlation coefficient of uv_x, where x is the cross-shelf coordinate, is derived that depends only on the sign of the bottom slope, the magnitude of friction, the local water depth and the forcing frequency. The momentum flux and Reynolds stress in the surface and bottom Ekman layers make a significant contribution to the mean flow. The Eulerian and Lagrangian mean flows have similar qualitative characteristics. The flow pattern is dependent on the type of forcing, coastal or interior, but in both cases the response is greatest at the free wave resonant frequencies. Along eastern boundaries, the mass transport for coastal forcing is equatorward, i.e., opposite to the direction of propagation of long, free shelf waves, at the mode 1 resonant frequency and poleward at the mode 2 resonant frequency, with magnitudes, for a wind stress of 1 dyn cm^{-2}, of -0.17×10^{12} and 0.11×10^{12} cm^3 s^{-1}, respectively. The mean alongshore velocities associated with these resonances are typically of order 1 cm s^{-1}. For interior forcing, the flow is poleward everywhere with a maximum near the shelf break. For a periodic oceanic velocity at the slope-interior junction with an amplitude of 1 cm s^{-1} the maximum alongshore mean flow and mass transport, at the first mode resonant frequency, are about 1 cm s^{-1} and 0.1×10^{12} cm^3 s^{-1}, respectively. The results for coastal forcing are inconsistent with observations of eastern boundary undercurrents, whereas the results for interior forcing are qualitatively consistent with the observations.

1. Introduction

Poleward undercurrents are a common feature at eastern ocean boundaries (Wooster and Reid, 1963). The undercurrents over the continental margin off California, Oregon and Peru are characterized by a core of poleward flowing water evidently of equatorial origin (Halpern *et al.*, 1978; Hickey, 1979, 1982; Brockmann *et al.*, 1980). The core is 20–50 km wide, 200–500 m in vertical extent, and situated near the shelf break. At present, no theory has adequately explained why poleward undercurrents are such a ubiquitous feature at eastern ocean boundaries.

Laboratory experiments by Caldwell and Eide (1976), Colin de Verdière (1979) and McEwan *et al.* (1980) have demonstrated that mean flows can be generated by oscillatory forcing in homogeneous, rotating fluids with a potential vorticity gradient due to variations in fluid depth. Outside of the forcing region, the mean flow generated is in the direction of long, free shelf wave propagation, i.e., retrograde. Colin de Verdière (1979) and McEwan *et al.* (1980) demonstrated experimentally that when the forcing travels in a retrograde sense the wave pattern is well ordered and the mean flow relatively strong, whereas, when the forcing travels prograde, the wave pattern is unsteady and the mean flow is weak.

In this paper we investigate the possibility that mean poleward undercurrents at eastern boundaries are forced by an oscillatory wind stress. Recent theoretical studies of mean flow generation are presented in Loder (1980) and Huthnance (1981, 1973), where references to previous studies are given. Huthnance (1973) and Loder (1980) obtained analytical expressions for the tidal-forced mean alongshore velocity in a homogeneous fluid over a sandbank by assuming that alongshore gradients are zero. Huthnance (1981) derives an expression for the mean flow generated over a shelf given the fluctuating velocities, parameterized bottom stress and vanishingly small friction. These results are not directly applicable to mean flows over continental margins forced by long-period (5–12 days) traveling wind stress since effects of a traveling forcing function, free wave resonances and a coastal boundary condition are not considered.

We solve for the mean flow in a homogeneous fluid over a continental slope with bottom friction by assuming the nonlinear terms are small and expanding the variables in powers of the Rossby number. A traveling wind stress is chosen such that the time mean

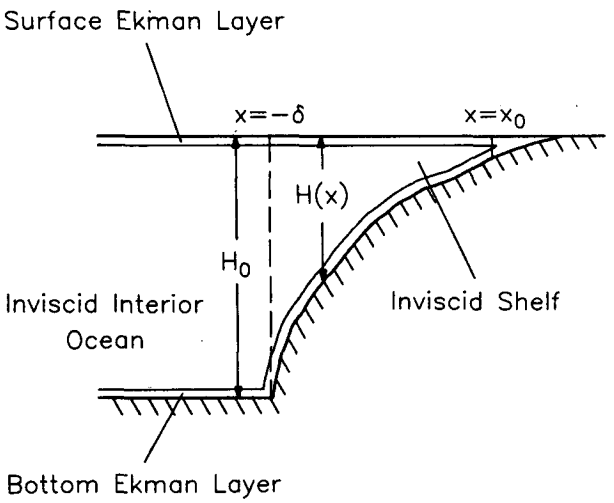

FIG. 1. Schematic of model geometry.

over a period is zero. Thus, the first-order variables have a zero time mean while the second-order variables provide the lowest order contribution to the mean flow. Frictional effects are retained at lowest order. The alongshore length scale is assumed to be greater than the cross-shelf length scale, i.e., a long-wave approximation (Allen, 1976) is made. This assumption simplifies the algebra and allows an analytical solution to the second-order mean flow in terms of the first-order variables. Several important results of the model, however, are found to be independent of the long-wave approximation.

2. Formulation

We consider an f-plane model utilizing a straight continental margin, with uniform alongshore topography, adjoining a flat bottomed ocean. The fluid is homogeneous and bottom friction is present. The fluid is assumed to be inviscid away from the surface and bottom boundary layers. Cartesian coordinates[1] (x', y', z') with corresponding velocity components (u', v', w') are used, where z' is vertical, positive upwards, x' is cross-shelf, positive onshore, and y' is alongshore.

The variables (u', v', w', p') and (x', y', z', t') are scaled by $(U, U, UH_0L^{-1}, Uf L\rho)$ and $(L, L, H_0, (\delta f)^{-1})$, respectively, where $U = \delta\tau_0(\delta_E\rho f H_0)^{-1}$ is a characteristic velocity, H_0 the depth of the interior ocean, L a characteristic alongshore length scale, f the Coriolis parameter, ρ the constant fluid density, $\delta_E = [\nu_T/(fH_0^2)]^{1/2}$ the dimensionless Ekman layer depth, δ the ratio of cross-shelf to alongshore length scales, τ_0 the characteristic wind stress, and ν_T the constant vertical turbulent eddy viscosity. The characteristic velocity U is chosen by assuming that the surface and bottom Ekman cross-shelf transports balance at the coast (see Section 5a). The Rossby number, $\tilde{\epsilon} = U(fL)^{-1}$, is assumed small such that a perturbation expansion may be made in the limit $\tilde{\epsilon} \to 0$. We assume the fluid is hydrostatic and bounded above by a rigid lid. In nondimensional variables, the governing equations are

$$\delta u_t + \tilde{\epsilon}(uu_x + vu_y + wu_z) - v = -p_x + \delta_E^2 u_{zz}, \quad (2.1a)$$

$$\delta v_t + \tilde{\epsilon}(uv_x + vv_y + wv_z) + u = -p_y + \delta_E^2 v_{zz}, \quad (2.1b)$$

$$0 = -p_z, \quad (2.1c)$$

$$u_x + v_y + w_z = 0, \quad (2.1d)$$

where the subscripts (x, y, z, t) denote partial differentiation.

An alongshore wind stress of the following form is assumed:

$$\tau = \sin(kx + \phi)\cos(ly - \omega t), \quad (2.2)$$

where k, l, ϕ and ω are respectively the cross-shelf and alongshore wavenumbers, an arbitrary phase, and the forcing frequency.

The model geometry (Fig. 1) has a rigid lid at $z = 0$, a variable depth bottom at $z = -H(x)$, a coast at $x = x_0$ $(x_0 \leq 0)$, and a flat bottom extending from $x = -\delta$ to $x \to -\infty$. The boundary conditions follow from the assumptions of an imposed alongshore wind stress at $z = 0$, a no-slip condition at $z = -H(x)$, no net mass transport into the coast at $x = x_0$, and a bounded solution as $x \to -\infty$. The resulting boundary conditions are

$$u_z = w = 0, \quad \delta_E v_z = \tau, \quad \text{at} \quad z = 0, \quad (2.3a)$$

$$u = v = w = 0, \quad \text{at} \quad z = -H(x), \quad (2.3b)$$

$$\int_{-H}^{0} u\,dz = 0, \quad \text{at} \quad x = x_0, \quad (2.3c)$$

$$u, v, w < \infty, \quad \text{as} \quad x \to -\infty. \quad (2.3d)$$

The domain is divided into four regions, inviscid shelf, surface Ekman layer, bottom Ekman layer and inviscid interior ocean. The variables in the last three of those four regions are denoted by the superscripts T, B and I, respectively. The interior ocean variables are matched to the shelf variables by requiring that pressure and onshore velocity be continuous at $x = -\delta$.

The momentum equations for the inviscid fluid on the shelf and in the interior ocean are

$$\delta u_t + \tilde{\epsilon}(uu_x + vu_y) - v = -p_x, \quad (2.4a)$$

$$\delta v_t + \tilde{\epsilon}(uv_x + vv_y) + u = -p_y, \quad (2.4b)$$

$$u_x + v_y + w_z = 0. \quad (2.4c)$$

The corresponding vorticity equation is

[1] Dimensional variables for which a nondimensional counterpart will be defined are marked with primes.

$$\delta(v_x - u_y)_t + \tilde{\epsilon}(uv_x + vv_y)_x - \tilde{\epsilon}(uu_x + vu_y)_y - w_z = 0. \quad (2.5)$$

a. Inviscid shelf

In the shelf region, the long-wave approximation, $\delta \ll 1$, is made. As a result, the shelf variables are expanded in the form

$$u = u_0 + \epsilon u_1 + \cdots, \quad (2.6a)$$

$$v = \delta^{-1}(v_0 + \epsilon v_1 + \cdots), \quad (2.6b)$$

$$w = \delta^{-1}(w_0 + \epsilon w_1 + \cdots), \quad (2.6c)$$

$$p = p_0 + \epsilon p_1 + \cdots, \quad (2.6d)$$

$$x = \delta\xi, \quad (2.6e)$$

where

$$\epsilon = \tilde{\epsilon}/\delta^2 = (U/\delta)/(f\delta L) \quad (2.6f)$$

is the Rossby number formed by the alongshore velocity scale U/δ and the cross-shelf length scale δL. We order the small parameters δ, δ_E and ϵ such that δ_E/δ, δ/ϵ and δ_E/ϵ are O(1) quantities. Substituting (2.6) into (2.4) we obtain at O(1),

$$v_0 = p_{0\xi}, \; v_{0t} + u_0 = -p_{0y}, \quad (2.7a, b)$$

$$u_{0\xi} + v_{0y} + w_{0z} = 0, \quad (2.7c)$$

and at O(ϵ),

$$v_1 = p_{1\xi}, \quad (2.8a)$$

$$v_{1t} + u_1 = -p_{1y} - (u_0 v_{0\xi} + v_0 v_{0y}), \quad (2.8b)$$

$$u_{1\xi} + v_{1y} + w_{1z} = 0. \quad (2.8c)$$

The time mean flow is obtained by applying a time average,

$$\langle(\ \ )\rangle = 1/T \int_{t_0}^{t_0+T} (\ \ )dt,$$

where $T = 2\pi/\omega$ and t_0 is arbitrary, to the O(ϵ) equations. The form of the forcing (2.2) implies additional simplifications, i.e., for all O(1) variables $\langle(\ \ )\rangle = 0$, and for all O(ϵ) variables $\langle(\ \ )_y\rangle = 0$.

The depth-integrated vorticity equations are formed by utilizing (2.6) with (2.5) and depth-integrating to obtain at O(1),

$$Hv_{0\xi t} - [w_0(z = 0) - w_0(z = -H)] = 0, \quad (2.9)$$

and at O(ϵ),

$$[\langle w_1(z = 0)\rangle - \langle w_1(z = -H)\rangle] = H\langle u_0 v_{0\xi}\rangle_\xi, \quad (2.10)$$

where $H = H(\xi)$. The vertical velocities w_0 and $\langle w_1\rangle$ at $z = 0$, $-H$ are obtained from the Ekman layer solutions (see Appendix A).

The boundary condition (2.3c) at the coast, $\xi = \xi_0$, is, for O(1),

$$H(\xi_0)u_0 + (\delta_E/\delta)\left(\int_{-\infty}^{0} \tilde{u}_0^T d\eta + \int_0^{\infty} \tilde{u}_0^B d\zeta\right) = 0, \quad (2.11)$$

and for O(ϵ),

$$H(\xi_0)\langle u_1\rangle + (\delta_E/\delta)\left(\int_{-\infty}^{0} \langle\tilde{u}_1^T\rangle d\eta + \int_0^{\infty} \langle\tilde{u}_1^B\rangle d\zeta\right) = 0, \quad (2.12)$$

where $\eta = z/\delta_E$ and $\zeta = (z + H)/\delta_E$ are the stretched vertical coordinates and $u^T = \tilde{u}^T/\delta$ and $u^B = \tilde{u}^B/\delta$ are rescaled velocities for the surface and bottom Ekman layers, respectively (see Appendix A).

b. Inviscid interior ocean

Boundary conditions for the shelf variables at the slope boundary, $\xi = -1$, are obtained by matching with the appropriate solution for the interior ocean. The interior ocean variables are expanded as

$$u^I = \delta^{-1}(u_0^I + \epsilon u_1^I + \cdots), \quad (2.13a)$$

$$v^I = \delta^{-1}(v_0^I + \epsilon v_1^I + \cdots), \quad (2.13b)$$

$$w^I = \delta_E\delta^{-1}(w_0^I + \epsilon w_1^I + \cdots), \quad (2.13c)$$

$$p^I = \delta^{-1}(p_0^I + \epsilon p_1^I + \cdots), \quad (2.13d)$$

Substituting (2.13) into (2.4) and collecting terms of O(1), we obtain

$$v_0^I = p_{0x}^I, \quad u_0^I = -p_{0y}^I, \quad (2.14a, b)$$

$$u_{0x}^I + v_{0y}^I = 0. \quad (2.14c)$$

The O(1) depth-integrated vorticity equation is formed by utilizing (2.13) with (2.5) and depth integrating to obtain

$$(v_{0x}^I - u_{0y}^I)_t - (\delta_E/\delta)[w_0^I(z = 0) - w_0^I(z = -1)] = 0. \quad (2.15)$$

We may write (2.15) in terms of pressure by utilizing (2.14), (A20) and (2.2) to obtain

$$\nabla_H^2 p_{0t}^I + \gamma\nabla_H^2 p_0^I = \sqrt{2}k\gamma \cos(kx + \phi)\cos(ly - \omega t), \quad (2.16a)$$

where $\nabla_H^2 = \partial^2/\partial x^2 + \partial^2/\partial y^2$ and

$$\gamma = \delta_E/(\sqrt{2}\delta). \quad (2.16b)$$

The conditions for matching the variables from the interior ocean and shelf are

$$p^I = p, \quad \text{at} \quad x = -\delta, \quad (2.17a)$$

$$\tilde{\epsilon}(u^I u_x^I + v^I u_y^I)_t + (\tilde{\epsilon}/\delta)(u^I v_x^I + v^I v_y^I) + \delta u_{tt}^I + p_{xt}^I = p_{xt} + \delta u_{tt} + (\tilde{\epsilon}/\delta)(uv_x + vv_y) + \tilde{\epsilon}(uu_x + vu_y)_t, \quad \text{at} \quad x = -\delta, \quad (2.17b)$$

Expanding p^I in a Taylor series about $x = 0$, and utilizing (2.6) and (2.13), we obtain at O(1),

$$p_0^I(x = 0) = 0, \tag{2.18a}$$

$$p_{0x}^I(x = 0) = p_{0\xi}(\xi = -1). \tag{2.18b}$$

The solution to (2.16) with (2.18a) and (2.3d) is,

$$p_0^I = -[\cos(kx + \phi) - e^{|l|x}\cos\phi]G(y, t), \tag{2.19a}$$

where

$$G(y, t) = \sqrt{2}k\gamma[(k^2 + l^2)(\omega^2 + \gamma^2)]^{-1} \times [\gamma\cos(ly - \omega t) - \omega\sin(ly - \omega t)]. \tag{2.19b}$$

The boundary condition on p_0 at $\xi = -1$, from (2.18b), is

$$p_{0\xi}(\xi = -1) = (k\sin\phi + |l|\cos\phi)G(y, t). \tag{2.20}$$

3. Analysis

The inviscid shelf motion is determined in three steps. First, the O(1) motion is solved numerically, which allows $H(\xi)$ to be an arbitrary function. Second, the O(ϵ) Eulerian time-mean solution is found analytically in terms of the O(1) solution. Finally, the Lagrangian mean flow is found by adding the Stokes drift to the O(ϵ) Eulerian mean flow.

a. O(1) *solution*

We solve the O(1) equations governing the shelf motions by writing (2.9) in terms of pressure. Substituting (A11) and (A17) into (2.9), and using (2.7), yields

$$Hp_{0\xi\xi t} + \gamma p_{0\xi\xi} + H_\xi(p_{0y} + p_{0\xi t}) = 0. \tag{3.1}$$

The boundary condition at the coast is expressed in terms of pressure by substituting (A10) and (A16) into (2.11):

$$p_{0\xi} = \sqrt{2}\sin\phi\cos(ly - \omega t) - H(\xi_0)\gamma^{-1}(p_{0y} + p_{0\xi t}), \quad \text{at} \quad \xi = \xi_0. \tag{3.2}$$

We employ a depth profile for which $H(\xi_0) < \sqrt{2}\gamma$ (see Table 1). Correspondingly, the second term on the right-hand side (RHS) of (3.2) is usually small compared to $p_{0\xi}$. When $H(\xi_0) < \sqrt{2}\gamma$ the surface Ekman transport is primarily compensated at the coast by a bottom Ekman layer transport. The velocity scaling used in this paper is appropriate for this depth profile.

A forced solution of the form

$$p_0 = \mathrm{Re}\{\psi(\xi)\exp[i(ly - \omega t)], \tag{3.3}$$

is sought where $\psi(\xi)$ is a complex function (see Appendix B).

b. O(ϵ) *solution*

The mean O(ϵ) onshore velocity is found by time averaging (2.8b), which gives

$$\langle u_1\rangle = -\langle u_0 v_{0\xi}\rangle. \tag{3.4}$$

The O(ϵ) mean vorticity equation [(2.10)] may be rewritten, utilizing (A13), (A19) and (3.4), as

$$-\sqrt{2}\gamma\langle\tau v_{0\xi\xi}\rangle - \gamma\langle v_{1\xi}\rangle + (7/20)\gamma\langle v_0 v_{0\xi}\rangle_\xi = (H\langle u_0 v_{0\xi}\rangle)_\xi. \tag{3.5}$$

The boundary condition at $\xi = \xi_0$ is found by substituting (A12), (A18) and (3.4) into (2.12):

$$-H\langle u_0 v_{0\xi}\rangle - \sqrt{2}\gamma\langle\tau v_{0\xi}\rangle - \gamma\langle v_1\rangle + (7/20)\gamma\langle v_0 v_{0\xi}\rangle = 0, \quad \text{at} \quad \xi = \xi_0. \tag{3.6}$$

Integrating (3.5) once with respect to ξ and applying (3.6), we obtain

$$\langle v_1\rangle = -H\gamma^{-1}\langle u_0 v_{0\xi}\rangle + (7/20)\langle v_0 v_{0\xi}\rangle - \sqrt{2}\langle\tau v_{0\xi}\rangle. \tag{3.7}$$

The O(ϵ) Eulerian mean shelf velocities in (3.4) and (3.7) are the lowest order contributions to the mean flow. By comparing (3.5) and (3.6), we note that the mean cross-shelf transport in the interior is balanced by a net cross-shelf transport in the Ekman layers.

Eqs. (3.4) and (3.7) may be expressed in more convenient forms. Multiplying (3.1) by $v_{0\xi}$ and time averaging, we obtain

$$\langle u_0 v_{0\xi}\rangle = \gamma H_\xi^{-1}\langle v_{0\xi}^2\rangle. \tag{3.8}$$

Squaring (3.1) and time averaging, we have

$$\langle u_0^2\rangle = [(H/H_\xi)^2\omega^2 + \gamma^2/H_\xi^2]\langle v_{0\xi}^2\rangle, \tag{3.9}$$

where the form of the forcing (2.2) has allowed the substitution,

$$\langle v_{0\xi t}^2\rangle = \omega^2\langle v_{0\xi}^2\rangle. \tag{3.10}$$

Finally, using (3.8), (3.9) and (3.4), we obtain

$$\langle u_1\rangle = -\gamma H_\xi(\gamma^2 + H^2\omega^2)^{-1}\langle u_0^2\rangle, \tag{3.11}$$

and using (3.4), (3.7), and (3.11), we find

$$\langle v_1\rangle = -HH_\xi(\gamma^2 + H^2\omega^2)^{-1}\langle u_0^2\rangle + (7/20)\langle v_0 v_{0\xi}\rangle - \sqrt{2}\langle\tau v_{0\xi}\rangle. \tag{3.12}$$

In terms of dimensional variables, (3.11) and (3.12) are

$$\langle u'\rangle \approx (\delta_E'/H')_{x'} \times \{f\sqrt{2}[(\omega'/f)^2 + \tfrac{1}{2}(\delta_E'/H')^2]\}^{-1}\langle u'^2\rangle, \tag{3.13}$$

and

$$\langle v'\rangle \approx -H'_{x'}\{fH'[(\omega'/f)^2 + \tfrac{1}{2}(\delta_E'/H')^2]\}^{-1}\langle u'^2\rangle + (7/20)f^{-1}\langle v'v'_{x'}\rangle - \sqrt{2}(\delta_E'\rho f^2)^{-1}\langle\tau' v'_{x'}\rangle, \tag{3.14}$$

respectively. The mean cross-shelf velocity (3.11) and the first term on the RHS of (3.12) may be determined from δ_E, H, H_ξ, ω, δ, and the variance of u_0. It may

be shown that (3.11) is independent of the long-wave approximation. Similarly the first term on the RHS of (3.12) is independent of the long-wave approximation, but the second and third terms on the RHS are not.

Combining (3.8) and (3.9) to form a correlation coefficient, we have

$$R(u_0, v_{0\xi}) = \langle u_0 v_{0\xi}\rangle(\langle u_0^2\rangle\langle v_{0\xi}^2\rangle)^{-1/2}$$
$$= \mathrm{sgn}(H_\xi)[1 + (H\omega/\gamma)^2]^{-1/2}, \quad (3.15)$$

where $\mathrm{sgn}(H_\xi) = H_\xi/|H_\xi|$. Writing u_0 and $v_{0\xi}$ as

$$u_0 = |u_0| \cos(ly - \omega t + \theta), \quad (3.16a)$$

$$v_{0\xi} = |v_{0\xi}| \cos(ly - \omega t + \phi), \quad (3.16b)$$

where $|u_0|$ and $|v_{0\xi}|$ are the magnitudes and where θ and χ the phases of u_0 and $v_{0\xi}$, respectively, and substituting (3.16) into (3.15) then yields

$$|\theta - \chi| = \cos^{-1}[1 + (H\omega/\gamma)^2]^{-1/2}. \quad (3.17)$$

The above expression implies that the phase difference between u_0 and $v_{0\xi}$ has a simple relationship that is independent of whether the driving is by wind stress at the coast or indirectly by interior ocean wind-stress curl, and is independent of the length scales of the forcing and the magnitude of H_ξ.

For a monotonically increasing depth in the offshore direction, i.e., $H_\xi < 0$, $\langle u_1\rangle$ will always be positive, i.e., onshore. Similarly, the first term on the RHS of (3.12) will be positive, i.e., make a contribution to the alongshore velocity in the direction of long, free wave propagation. The second and third terms, however, can be either positive or negative depending on the profile of v_0. For the cases investigated in this paper, the boundary condition at the coast [(3.2)] and the interior ocean-continental margin matching condition [(2.20)] will tend to produce a profile of v_0 that is large at the coast and zero at $\xi = -1$, i.e., $v_0 v_{0\xi} > 0$. Thus, the second term will normally make a positive contribution and the third term a negative contribution. The sign of the alongshore velocity (3.12) will therefore depend on the relative magnitudes of the three terms.

c. *Lagrangian mean flow*

The alongshore Lagrangian mean flow (particle drift velocity) is the alongshore Eulerian mean flow plus the alongshore component of the Stokes drift (Longuet-Higgins, 1969), i.e.,

$$v_L = \langle v\rangle + v_S, \quad (3.18)$$

where the Stokes drift with scaling (2.6) is given approximately by

$$v_S = \epsilon\left\langle \int^t u_0 dt v_{0\xi} + \int^t v_0 dt v_{0y} \right\rangle + O(\epsilon^2), \quad (3.19)$$

and where $\int^t dt$ indicates an indefinite time integral.

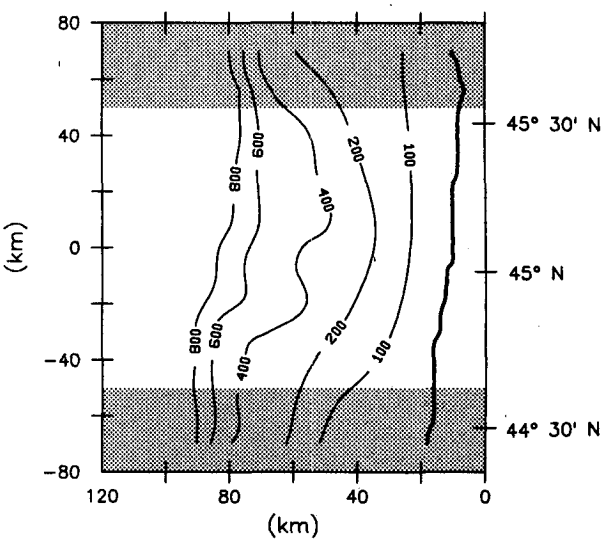

FIG. 2. Oregon continental margin topography from Peffley and O'Brien (1976). Contour interval is in meters. Nonshaded region denotes extent of alongshore averaging for the depth profile $H(\xi)$.

Thus, the Stokes drift velocity is the same order as the alongshore Eulerian mean flow (3.12).

Following a procedure similar to that used to derive (3.12) we find

$$v_{1S} = HH_\xi(\gamma^2 + H^2\omega^2)^{-1}\langle u_0^2\rangle + (l/\omega)\langle v_0^2\rangle. \quad (3.20)$$

Substituting (3.20) and (3.12) into (3.18) we have

$$v_{1L} = (7/20)\langle v_0 v_{0\xi}\rangle - \sqrt{2}\langle \tau v_{0\xi}\rangle + l/\omega\langle v_0^2\rangle, \quad (3.21)$$

which in dimensional variables is

$$v'_L \approx (7/20)f^{-1}\langle v'v'_{x'}\rangle - \sqrt{2}(\delta'_E \rho f^2)^{-1}\langle \tau' v'_{x'}\rangle + (l'/\omega')\langle v'^2\rangle. \quad (3.22)$$

d. *Topography*

The bottom topography used in the model, $H(\xi)$, is an alongshore averaged depth profile from the Oregon continental margin. Digitized topography (Peffley and O'Brien, 1976) was smoothed, then averaged over an alongshore distance of 100 km to produce a smooth profile (Fig. 2). An exponential tail was fitted to the profile to extend the depth from 1000 m, the maximum depth of the digitized data, to 2000 m, the interior ocean depth. The above procedure produced a depth profile that is smooth, continuous and monotonically increasing with distance offshore (Fig. 3).

e. *Forcing*

The wind stress [(2.2)] can force the inviscid shelf motion by two separate mechanisms, coastal forcing, where the shelf currents are driven by the boundary conditions at $\xi = \xi_0$ [(3.2)] ($\phi = \pi/2$, $k = 0$), and wind-stress curl forcing, where the shelf currents are

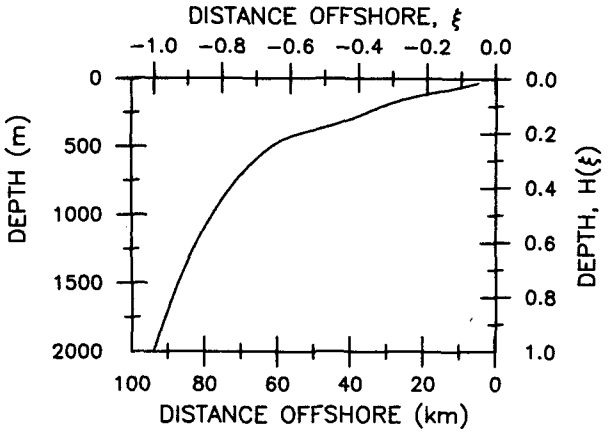

FIG. 3. Depth profile $H(\xi)$ as a function of distance offshore.

driven by the boundary condition at $\xi = -1$ [(2.20)] ($\phi = 0$, $k = 2\pi$).

We have found that the wind-stress curl forced response, for reasonable values of τ_0, is small relative to the coastal forced response. For a given τ_0, wind-stress curl forcing generates an O(1) alongshore velocity at $\xi = -1$ whose magnitude varies inversely with frequency (2.20). To help clarify the nature of the response on the continental margin to interior forcing, rather than holding τ_0 constant we vary τ_0 with frequency such that the magnitude of the oceanic velocity at $\xi = -1$ is fixed at v^I ($x = -1$) $= V$ (where $V' = 1$ cm s^{-1}).

We have found that when $\omega/l < 0$, i.e., for either the coastal or interior forcing traveling in the direction opposite to that of long, free waves, the response away from a narrow horizontal boundary layer at $\xi = \xi_0$ is $\sim 10^{-2}$ times the response for $\omega/l > 0$. Consequently, ω and l are limited to values such that $\omega/l > 0$.

4. Analytical example

The O(1) depth-integrated vorticity equation (3.1) may be solved analytically for the two-dimensional case where $(\ )_y = 0$ for all variables. We may then obtain analytical expressions for the O(1) velocities and the O(ϵ) mean alongshore velocity for arbitrary $H(\xi)$.

The O(1) vorticity equation (3.1) with the above assumption, may be written as

$$(Hv_{0t} + \gamma v_0)_\xi = 0. \tag{4.1}$$

Similarly, the boundary condition at the coast, $\xi = \xi_0$, becomes

$$Hv_{0t} + \gamma v_0 = \sqrt{2}\gamma \cos(\omega t), \quad \text{at} \quad \xi = \xi_0, \tag{4.2}$$

where a wind stress,

$$\tau = \cos(\omega t), \tag{4.3}$$

consistent with the above assumption is used.

The forced solution to (4.1) with the boundary condition (4.2) is

$$v_0 = \sqrt{2}\gamma[(\omega H)^2 + \gamma^2]^{-1} \times [\omega H \sin(\omega t) + \gamma \cos(\omega t)]. \tag{4.4}$$

The boundary condition at $\xi = -1$ [(2.20)] with the wind-stress (4.3) ($l \equiv 0$, $k \to 0$) is also satisfied by (4.4). The O(1) cross-shelf velocity, from (2.7b) and (4.4), is

$$u_0 = -\sqrt{2}\gamma\omega[(\omega H)^2 + \gamma^2]^{-1} \times [\omega H \cos(\omega t) - \gamma \sin(\omega t)]. \tag{4.5}$$

The above expressions for u_0 and v_0 satisfy (3.15).

The expression for the O(ϵ) Eulerian alongshore mean velocity [(3.7)] may be simplified by utilizing (2.7b), (4.1) and (4.2), to yield

$$\langle v_1 \rangle = -(13/20)\langle v_0 v_{0\xi} \rangle. \tag{4.6}$$

Substituting (4.4) into (4.6) yields

$$\langle v_1 \rangle = (13/20)\gamma^2\omega^2 H H_\xi [(\omega H)^2 + \gamma^2]^{-2}, \tag{4.7a}$$

which in dimensional variables is

$$\langle v' \rangle \approx \frac{13}{40} \frac{\tau'^2(\omega'/f)^2 H'_{x'}}{H'^3 f^3 \rho^2 [(\omega'/f)^2 + \frac{1}{2}(\delta'_E/H')^2]^2}. \tag{4.7b}$$

Similarly, we find the Lagrangian mean flow by utilizing (4.3), (4.4), and (4.7) with (3.21), to obtain

$$v_{1L} = (33/13)\langle v_1 \rangle. \tag{4.8}$$

For vanishingly small friction, i.e., in the limit $\delta'_E \to 0$, Eq. (4.7b) becomes

$$\lim_{\delta'_E \to 0} \langle v' \rangle \approx (13/40)\tau'^2 H'_{x'} (H'^3 f \rho^2 \omega'^2)^{-1}. \tag{4.9}$$

Thus, in the limit, $\delta'_E \to 0$, the Eulerian and Lagrangian alongshore mean velocities are nonzero (see Section 5a).

The O(1) alongshore velocity, for a forcing period of 5–12 days and a wind stress $\tau_0 = 1.0$ dyn cm^{-2}, has a maximum amplitude of ~ 25 cm s^{-1} at $\xi = \xi_0$ and decays to $\leqslant 1$ cm s^{-1} at $\xi = -1$. The cross-shelf velocity has an amplitude that is $\delta\omega = 0.06$ times the alongshore velocity.

The mean Eulerian and Lagrangian alongshore velocities, for the depth profile used here ($H_\xi < 0$), are negative everywhere, i.e., opposite to the direction of propagation of long, free shelf waves. The mean Eulerian velocity has a maximum of -0.8 cm s^{-1} at $\xi = \xi_0$ and decays quickly offshore. The magnitude at the shelf break, i.e., the 200 m isobath, is less than -0.05 cm s^{-1}. Thus, the flow is restricted to a negative jet at the coast with negligible velocities offshore.

A relationship between the nonlinear interactions that occur in the surface and bottom Ekman layers and the interior may be inferred from the fact that the depth-integrated cross-shelf velocity $\int_{-H}^{0} u dz$ is

zero for all ξ. Consequently, we can write the $O(\epsilon)$ depth-integrated cross-shelf velocities, utilizing (3.4), (A8b) and (A15b), as

$$\int_{-H}^{0} u dz = 0 = -(\delta_E/\delta)\Big[\langle v_{1\zeta}^B(\zeta = 0)\rangle + \int_0^\infty (\langle u_0^B v_{0\xi}^B\rangle - \langle v_{0\zeta}^B \int_0^\zeta u_{0\xi}^B d\zeta'\rangle) d\zeta\Big] - \Big\langle v_{0\xi}\Big[Hu_0 + (\delta_E/\delta)\Big(\int_0^\infty u_0^B d\zeta + \int_{-\infty}^0 u_0^T d\eta\Big)\Big]\Big\rangle . \quad (4.10)$$

The condition $\int_{-H}^0 u dz = 0$ also implies that the last term in (4.10) is identically equal to zero, so that

$$\langle v_{1\zeta}^B(\zeta = 0)\rangle = -\int_0^\infty \Big(\langle u_0^B v_{0\xi}^B\rangle - \langle v_{0\zeta}^B \int_0^\zeta u_{0\xi}^B d\zeta'\rangle\Big) d\zeta. \quad (4.11)$$

When the bottom Ekman layer results (A8), (A10) and (A12) are utilized (4.11) reduces to (4.6). Thus, the contribution to the alongshore mean flow $\langle v_1\rangle$ from the interior is *canceled* by the contributions from the surface and bottom Ekman layers and $\langle v_1\rangle$ is forced by the remaining terms from the bottom Ekman layer. This result demonstrates that the mean flows generated by interactions within the surface and bottom boundary layers can make a contribution as important to the mean alongshore flow as those in the interior.

The mean Eulerian velocity for this example is negative everywhere, whereas the observed mean alongshore velocities at eastern boundaries are positive (Wooster and Reid, 1963). The two-dimensional case, however, has the primary deficiency that the dominant response to forcing at the free shelf wave resonances cannot be investigated.

5. Discussion

a. *Frictional effects*

The existence of friction is necessary to obtain nonzero values of $\langle u_0 v_{0\xi}\rangle$ the forcing term in the time averaged $O(\epsilon)$ momentum equations. Once the solution is obtained, the limiting case $\delta_E' \to 0$ may be examined.

In the limit, $\delta_E' \to 0$, (3.13) becomes

$$\lim_{\delta_E' \to 0} \langle u'\rangle \approx 0. \quad (5.1)$$

Since $\langle u_0 v_{0\xi}\rangle$ goes to zero as $\delta_E' \to 0$ [(3.8)], the above result is expected. However, a nonzero limit is obtained in (3.14):

$$\lim_{\delta_E' \to 0} \langle v'\rangle \approx -H_{x'} f (H'\omega'^2)^{-1} \langle u'^2\rangle + (7/20) f^{-1} \langle v' v'_{x'}\rangle - T(x, y, t), \quad (5.2a)$$

which equivalently is

$$\lim_{\delta_E' \to 0} \langle v'\rangle \approx -H' H'_{x'} \Big[f \Big\langle \Big(\int^{t'} u' dt'\Big)^2 \Big\rangle - (7/20) \Big\langle v' \int^{t'} u' dt' \Big\rangle \Big] - T(x, y, t), \quad (5.2b)$$

where (3.1), with $\delta_E' \to 0$, has been utilized and

$$T(x, y, t) = \lim_{\delta_E' \to 0} \sqrt{2} (\delta_E' \rho f^2)^{-1} \langle \tau' v'_{x'}\rangle. \quad (5.3)$$

The term T in (5.3) is finite since the component of $v'_{x'}$ that is in phase with τ' is proportional to δ_E' (Brink and Allen, 1978). Similarly, the Lagrangian mean flow [(3.22)] may be written as

$$\lim_{\delta_E' \to 0} v_L' \approx (7/20) f^{-1} \langle v' v'_{x'}\rangle + l'/\omega' \langle v'^2\rangle - T(x, y, t). \quad (5.4)$$

The nonzero value of $\lim_{\delta_E' \to 0} \langle v'\rangle$ may be explained with reference to the boundary condition at $\xi = \xi_0$ [(2.10)]. The $O(\epsilon)$ interior onshore transport $H\langle u_1\rangle \approx H\delta_E \langle u_0^2\rangle$, which scales with δ_E, and the surface Ekman layer transport $\approx \delta_E \langle u_1^T\rangle$ are balanced by a *transport* in the bottom Ekman layer at $\xi = \xi_0$, which also scales with δ_E, i.e., $H(\xi_0)\langle u_1\rangle + \delta_E \langle u_1^T\rangle \approx \delta_E \langle u_1^B\rangle$. Thus, the *velocity* in the bottom Ekman layer, $\langle u_1^B\rangle$, has a component independent of δ_E, and since $\langle v_1\rangle \approx \langle u_1^B\rangle + \cdots$ [(A12)], $\langle v_1\rangle$ also has a component independent of δ_E.

A bottom boundary layer must satisfy two conditions for the limits (5.2) and (5.4) to hold. First, the stress in the layer must be proportional to v_1, i.e., $\tau = r(v + \cdots)$, where r is a "resistance coefficient." Second, the transport in the layer must also be proportional to v, i.e.,

$$\int_0^{z_0} u_1^B dz = rK(v + \cdots),$$

where z_0 is the top of the layer and K a constant independent of r. These conditions are satisfied when the bottom boundary layer is an Ekman layer. Bulk or slab layers based on Ekman dynamics should also give similar results.

The characteristic velocity used in Section 2 is inappropriate in the limit, $\delta_E \to 0$, since $\lim_{\delta_E \to 0} U \to \infty$. A general characteristic velocity valid in this limit is determined by balancing the three terms in (3.2):

$$U = \tau_0 [(\delta_E/\delta + H(\xi_0)) H_0 \rho f]^{-1}. \quad (5.5)$$

The appropriate characteristic velocity for $\delta_E \to 0$, from (5.5), is

$$U = \tau_0 [H'(x_0') \rho f]^{-1}, \quad (5.6)$$

which is the characteristic velocity normally associated with forced inviscid shelf models.

TABLE 1. Summary of parameter values.

f	$= 10^{-4}$ s^{-1}	l	$= 2\pi$
H_0	= 2 km	k	= 0
L	$= 10^3$ km	ϕ	$= \pi/2$
ρ	= 1 g cm^{-3}	δ	= 0.094
τ_0	= 1 dyn cm^{-2}	ξ_0	= −0.05
δ'_E	= 4 m	$H(\xi_0)$	= 0.0169
δ_E	= 0.002	$H'(\xi_0)$	= 33.8 m

b. *Coastal forced results*

The results for the coastal forced case were calculated numerically following the procedure outlined in Appendix B with the parameter values given in Table 1. The dimensional magnitude of the alongshore wind stress, $\tau' = \tau_0 \cos(ly - \omega t)$, is chosen so the maximum value $\tau_0 = \tau'_m = 1$ dyn cm^{-2}. The results presented here may be extended to other values of τ'_m, i.e., τ^*, by multiplying the O(1) alongshore velocity v'_0 by τ^*/τ'_m and the Eulerian and Lagrangian mean velocities $\langle v' \rangle$ and v'_L by $(\tau^*/\tau'_m)^2$.

• O(1) ALONGSHORE VELOCITY

The amplitude and phase of the O(1) alongshore velocity, $v_0 = |v_0| \cos(ly - \omega t + \chi)$ are plotted as functions of ξ and the parameter $\alpha = \omega'/f = \delta\omega$ in Fig. 4.

The O(1) alongshore velocity amplitude response has two local maxima which correspond to the mode 1 resonant response at $\alpha = 0.24$ and the mode 2 resonant response at $\alpha = 0.06$. A maximum amplitude of ~35 cm s^{-1} occurs at $\xi = \xi_0$ for $\alpha = 0.24$, i.e., the mode 1 resonant frequency. There are two maxima associated with the mode 2 resonant response. A maximum of ~5 cm s^{-1} at $\xi = -0.7$ and ~25 cm s^{-1} at the coast, $\xi = \xi_0$.

The O(1) alongshore velocity phase, referenced to the wind stress, has its largest change with frequency at a resonance. At the mode 1 resonance the phase is nearly constant cross-shelf, equal to −6° at $\xi = \xi_0$ and 0° at $\xi = -1$ so that nearshore fluctuations lead those offshore. This compares with a 22° phase difference in the same sense for a free wave (Appendix C). At the mode 2 resonant frequency, the phase is 0° at $\xi = \xi_0$, −180° at $\xi = -1$, with 97% of the cross-shelf phase difference occurring between $\xi = \xi_0$ and −0.5, where offshore fluctuations lead those nearshore.

• EULERIAN MEAN FLOW

The Eulerian and Lagrangian mean alongshore velocities, $\langle v' \rangle$ and v'_L, are plotted as functions of ξ and α in Fig. 5. Eulerian and Lagrangian mean velocity profiles are plotted as a function of ξ for different values of α in Fig. 6.

The Eulerian mean velocity response, in general, has two frequency regimes, a resonant and an off-resonant response (Fig. 5). The mode 1 resonant response ($\alpha = 0.24$) has a positive jet of ~1 cm s^{-1} at $\xi = \xi_0$ and a negative maximum of ~ −0.5 cm s^{-1} at $\xi = -0.8$ (Fig. 6). At the mode 2 resonant frequency, a maximum of ~ −0.5 cm s^{-1} is located at $\xi = -0.85$ and a coastal jet is absent. The off-resonant response consists of a jet of ~ −1 cm s^{-1} near $\xi = \xi_0$.

The Eulerian and Lagrangian integrated mass transports,

$$M_E = \int_{-\delta L}^{x'_0} H\langle v' \rangle dx' \quad \text{and} \quad M_L = \int_{-\delta L}^{x'_0} H v'_L dx', \quad (5.7)$$

are plotted as functions of α in Fig. 7. The magnitude of the alongshore mean transport in the surface and bottom Ekman layers is the order of $\gamma/H(\xi)$ times the shelf contribution $\langle v_1 \rangle$. This is a small correction, except near $\xi = \xi_0$, and has been ignored.

The large peaks in mass transport occur at the free wave resonances. The offshore velocity maxima in deep water are the principle cause for the mass transport peaks. Although the highest velocities occur away from a resonance, these maxima are near the

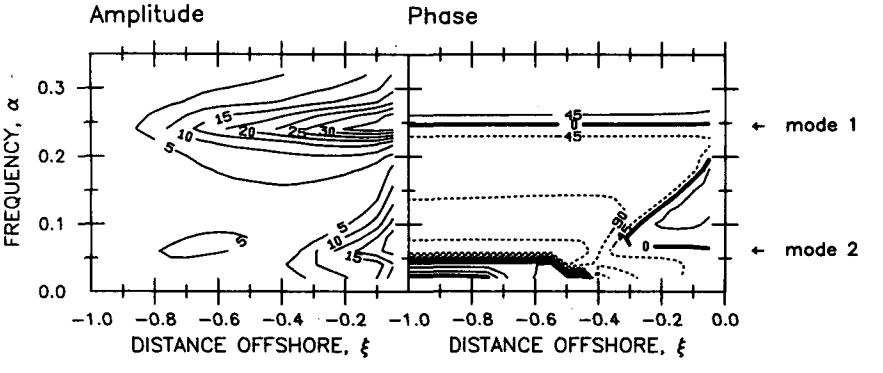

FIG. 4. Amplitude (left) and phase (right) of coastal forced O(1) alongshore velocity as functions of ξ, distance offshore, and $\alpha = \omega'/f$, a nondimensional forcing frequency. The amplitude contours are isotachs (5 cm s^{-1} contour interval) and phase contours are lines of constant phase (45° contour interval).

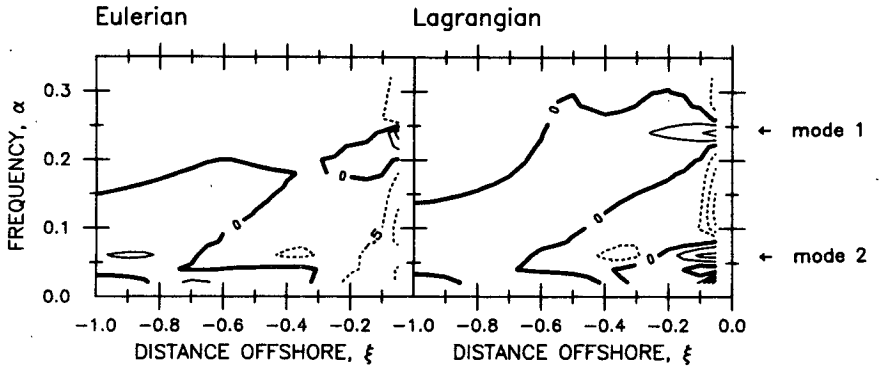

FIG. 5. Coastal forced alongshore mean velocity as a function of ξ and $\alpha = \omega'/f$. The contours are isotachs (cm s^{-1}); the double weight contour is the zero velocity level. The free wave resonant frequencies for the first two modes are marked. Eulerian $\langle v' \rangle$ (contour interval = 0.5 cm s^{-1}) and Lagrangian v'_L (contour interval = 1 cm s^{-1}) alongshore mean velocities are displayed to the left and right, respectively. The dotted and solid contours correspond to negative and positive values, respectively.

coast in shallow water and the resultant mass transport is small relative to the mass transport at resonance. A sign change in mass transport occurs near $\alpha = 0.16$; the transport is negative for mode 1 and positive for mode 2. The maximum negative transport of $\sim -0.2 \times 10^{12}$ cm^3 s^{-1}, associated with mode 1, is approximately twice the maximum positive transport of $\sim 0.1 \times 10^{12}$ cm^3 s^{-1}, associated with mode 2.

• LAGRANGIAN MEAN FLOW

The Lagrangian response has two frequency regimes that are similar to those in the Eulerian response (Fig. 5). The Lagrangian resonant response is also characterized by a positive coastal jet of 2 cm s^{-1} at the mode 1 and mode 2 resonant frequencies. In general, the Lagrangian response has larger regions of positive flow over the shelf.

The Lagrangian and Eulerian mean alongshore flows (Fig. 6) are nearly identical from the interior ocean-continental margin junction to the 400 m isobath ($\xi = -0.6$), i.e., the Stokes drift v_S is small in deep water. The Stokes drift is larger than the Eulerian mean flow inshore of the 400 m isobath.

The Lagrangian alongshore mass transport shown in Fig. 7 is not qualitatively different from the Eulerian mass transport. The principle differences occur at lower frequencies, i.e., $\alpha \leq 0.05$. The peaks in the mass transport are caused by the resonant responses with the main contribution coming from the alongshore velocities offshore of the 200 m isobath.

The frequencies at which resonance occurs are dependent on several parameters. These parameters either have a large natural variation, e.g., the shelf width, or are not well known, e.g., the atmospheric length scales of τ. We can expect that given a forcing function with a reasonably smooth wavenumber–fre-

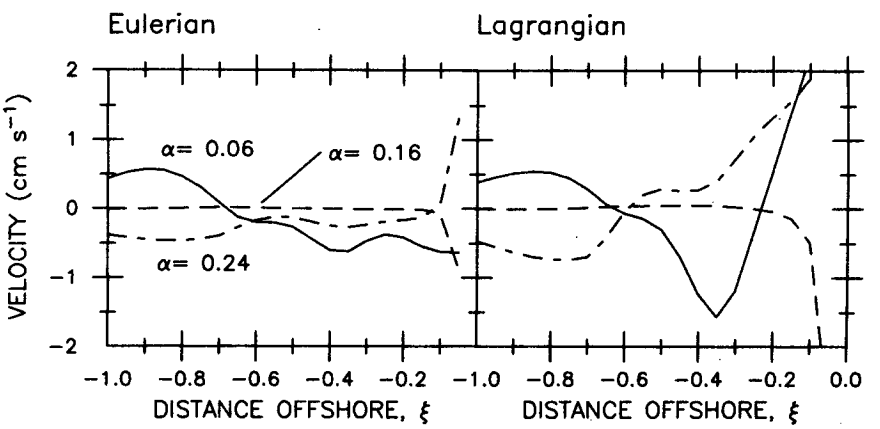

FIG. 6. The dimensional Eulerian (left) and Lagrangian (right) coastal forced alongshore velocity v' as a function of ξ, distance offshore. The dot-dashed, solid and dashed lines correspond to mode 1 ($\alpha = \omega'/f = 0.24$) and 2 ($\alpha = 0.06$) resonant frequencies, and a non-resonant ($\alpha = 0.16$) frequency, respectively. The nonresonant frequency is chosen such that the Eulerian mass transport is a minimum.

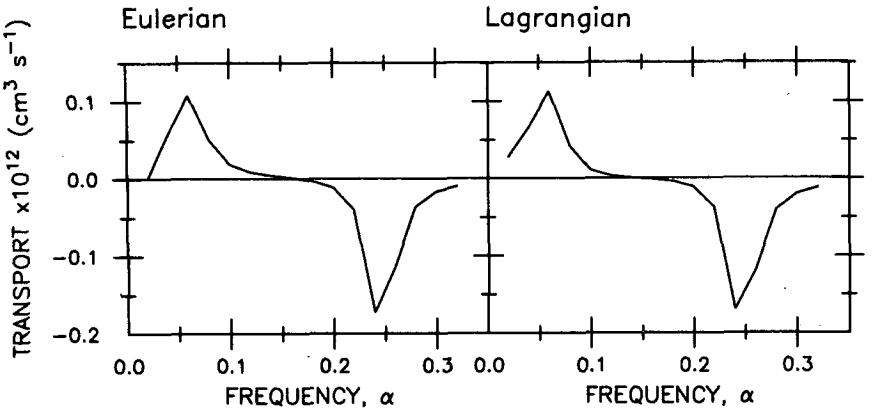

FIG. 7. Eulerian (left) and Lagrangian (right) coastal forced mass transport as a function of $\alpha = \omega'/f$. Transport is in 10^{12} cm^3 s^{-1}.

quency spectrum the resonant response will dominate.

c. *Interior forced results*

The results for the interior forced case were calculated numerically by varying τ_0 with frequency (Section 3e) and applying the procedure described in Appendix B. A dimensional magnitude for the imposed alongshore oceanic velocity V' of 1 cm s^{-1} is used. The results presented may be extended to other values of V', i.e., V^*, by multiplying the O(1) alongshore velocity v_0' by V^*/V' and the Eulerian and Lagrangian mean velocities by $(V^*/V')^2$.

• O(1) ALONGSHORE VELOCITY

The O(1) alongshore velocity amplitude response is similar to the coastal forced response (Fig. 4). The response is negligible away from the resonant frequencies. A maximum of 30 cm s^{-1} at $\xi = -0.1$ is associated with the mode 1 resonance, $\alpha = 0.24$, and a maximum of 3 cm s^{-1} occurs at the mode 2 resonant frequency, $\alpha = 0.06$. The mode 2 resonant response for interior forcing has a single maximum at $\xi = -0.1$.

The O(1) alongshore velocity phase, referenced to the imposed oceanic velocity V, rapidly decreases from 0° at $\xi = -1$ to −120° at $\xi = -0.8$ and remains nearly constant until $\xi = -0.2$ where the phase decreases to −135° at $\xi = \xi_0$, for the mode 1 resonant response. The phase associated with the mode 2 resonant response decreases monotonically, with a nearly constant slope, from 0° at $\xi = -1$ to +45° at $\xi = \xi_0$, going through a value of −180° at $\xi = -0.4$.

• EULERIAN MEAN FLOW

The interior forced Eulerian and Lagrangian mean alongshore velocities, $\langle v' \rangle$ and v_L', are plotted in Fig. 8 as functions of distance offshore ξ and frequency α.

The Eulerian velocity is positive, i.e., in the direction of propagation of long, free shelf waves, everywhere, in contrast to the coastal forced mean flow. The velocity response has two frequency regimes, a resonant and an off-resonant response. The resonant response has a magnitude that is several times larger

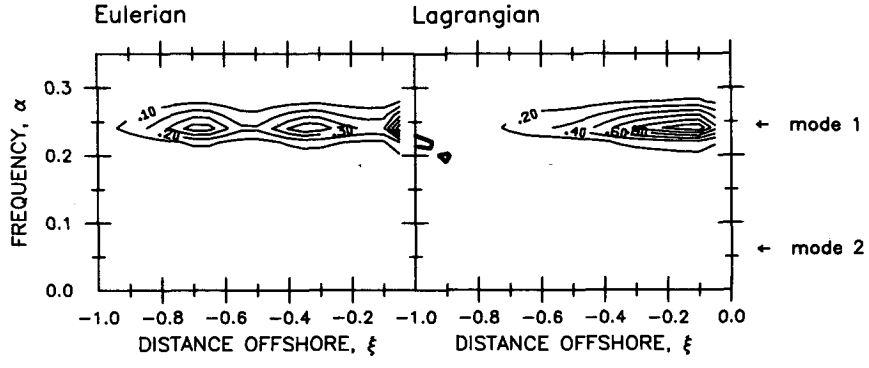

FIG. 8. Interior forced alongshore mean velocity as a function of ξ and $\alpha = \omega'/f$. Notation is the same as for Fig. 5 (contour interval is 0.1 cm s^{-1} for Eulerian and 0.2 cm s^{-1} for Lagrangian).

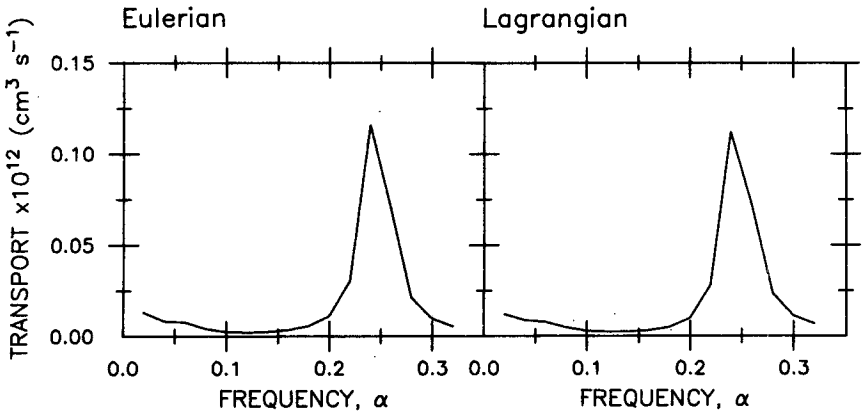

FIG. 9. Eulerian (left) and Lagrangian (right) interior forced mass transport as a function of $\alpha = \omega'/f$. Transport is in 10^{12} cm^3 s^{-1}.

than the off-resonant response and a maximum that usually occurs near the shelf break ($\xi = -0.3$), i.e., the 200 m isobath. A narrow positive jet, situated between $\xi = \xi_0$ and -0.1, occurs at the mode 1 resonant frequency.

The mode 1 resonant response has two maxima of 0.4 cm s^{-1} occurring at $\xi = -0.3$ and -0.7, i.e., the 200 and 600 m isobaths, respectively. A break in slope (Fig. 3) is associated with each maximum. The response at the mode 2 resonance is negligible relative to the mode 1 response.

The Eulerian alongshore mass transport shown in Fig. 9 has maxima occurring at the free wave resonances. The transport at the mode 1 resonance is $\sim 0.1 \times 10^{12}$ cm^3 s^{-1}.

• LAGRANGIAN MEAN FLOW

The Lagrangian mean velocity is primarily positive and has its largest values at the free wave resonances. The response associated with the mode 1 resonance is larger than the mode 2 response. In general, the maxima at a resonance are inshore of the shelf break.

The mode 1 resonant response is a single maximum of 1.3 cm s^{-1} at $\xi = -0.15$. The response extends offshore of $\xi = -0.4$, where the magnitude has dropped to 0.8 cm s^{-1}. A relatively small response, associated with the mode 2 resonance, of 0.1 cm s^{-1} occurs at $\xi = -0.15$.

The Eulerian and Lagrangian mass transports are nearly identical. The Lagrangian transport is typically 97% of the Eulerian transport.

d. Comparison with other theory

Mean flow generation in a homogeneous fluid over a shelf was studied by Huthnance (1981; henceforth referred to as H). Small-amplitude oscillations and weak friction were assumed. A solution was found by assuming the Rossby number small and expanding in Rossby number. An expression for the mean alongshore velocity $\langle v_1 \rangle$ given an incident oscillatory current, parameterized bottom stress ($\tau^B = rv$), and infinitesimal friction was derived in H [his (5.2)].

We may compare (5.2) in H with (5.2b) here by including in the former the bottom boundary layer momentum flux term neglected in the derivation of (5.2) [that term is in the paragraph containing (2.3) in H], and a uniform eddy viscosity model, i.e., a bottom Ekman layer. The alongshore bottom stress, for an Ekman layer, is, for O(1),

$$\tau_0^B = rv_0, \tag{5.8a}$$

where r is a "resistance" coefficient, and for O(ϵ),

$$\langle \tau_1^B \rangle = r\left[\langle v_1 \rangle + (3/20)H^{-1}H_\xi \left\langle v_0 \int^t u_0 dt \right\rangle\right]. \tag{5.8b}$$

Substituting the above expressions for the bottom stress (5.8a, b) into (3.8) in H we obtain

$$\langle v_1 \rangle = -H^{-1}H_\xi\left[\left\langle \left(\int^t u_0 dt\right)^2 \right\rangle - (7/20)\left\langle v_0 \int^t u_0 dt \right\rangle\right], \tag{5.9}$$

which replaces (5.2) in H.

If we assume that no alongshore gradients exist, then (5.9) may be written as

$$\langle v_1 \rangle = (27/40)\left\langle \left(\int^t u_0 dt\right)_\xi^2 \right\rangle, \tag{5.10}$$

which is identical to the result given in the paragraph following (5.5) in H, where similar assumptions and bottom stress are used. For no alongshore gradients, Eq. (5.2) in H is

$$\langle v_1 \rangle = \left\langle \left(\int^t u_0 dt\right)_\xi^2 \right\rangle. \tag{5.11}$$

Comparing (5.10) and (5.11) above, we see, for no alongshore gradients that the derived alongshore

mean flow is 1.48 times larger if, as in H (5.2), the bottom layer momentum flux term is neglected and a parameterized bottom stress, $\tau^B = rv$, is assumed.

A linear model of the wind-forced viscous flow near a continental boundary that retained finite thickness surface and bottom Ekman layers was developed by Spillane (1980). The model makes use of a homogeneous fluid, alongshore invariant topography, and a spectral form for the wind stress.

To assess the effects of a finite coastal wall at $\xi = \xi_0$ [(3.2)], the O(1) results obtained here were compared with those from the Spillane model in which the inclusion of vertical gradients in the analysis allows a coastal wall height $H(\xi_0)$ of zero. The present model was run with the topography used by Spillane. Excellent agreement between the sea surface elevation from his model [$H(\xi_0) = 0$] and the O(1) pressure here was found for values of $H'(\xi_0)$ from 0 to 34 m. This insensitivity to the value of wall height was also found by Spillane, i.e., for $H(\xi_0) \leq \sqrt{2}\gamma$ the flow offshore of the boundary was unchanged.

e. *Comparison with observations*

Evidence for a relatively narrow core of poleward flow off southern Washington was presented by Hickey (1979). The mean flow was observed from current measurements taken from July to September 1972 at 46°N. The core was found to be 20 km wide with a maximum velocity of 16 cm s^{-1}. The core occurred at mid-depth in 600 m of water.

The present model demonstrates that forced barotropic shelf waves with bottom friction can, through nonlinear interactions, generate a mean flow with non-negligible amplitudes. The mean flow generated has a response that is frequency-dependent, and a maximum alongshore mass transport at the free wave resonant frequencies. The predominant sign of the mean alongshore velocity depends on the forcing type used.

The mean flow generated by coastal forcing is usually equatorward, i.e., in a direction opposite to the direction of propagation of long, free shelf waves, whereas, the undercurrents at eastern boundaries are observed to be poleward. For this forcing, offshore poleward flows are found only in connection with the mode 2 resonance (see Fig. 5). This flow is offshore at the 200 m isobath with a width of 5–20 km.

For interior forcing, the mean flow generated is poleward, although the magnitude is generally smaller than the coastal forced mean currents. The largest response occurs at the mode 1 resonant frequency. The core of poleward flow is usually centered over the shelf break and has a width of ~20 km.

6. Summary

The generation of a mean flow over a continental margin by the self interaction of long, forced shelf waves has been studied. In the presence of dissipation provided by bottom friction, the interaction generates a mean flow. The physical reason for the existence of the alongshore mean velocity can be seen from the vertically integrated vorticity balance (2.10). The local mean vorticity change generated by $\langle u_0 v_{0\xi} \rangle_\xi$, the net transport of potential vorticity, is equal to the stretching caused by the difference in the mean vertical velocity at the surface and bottom boundaries. The above net vorticity transport is nonzero when friction is present, i.e., when $\gamma \neq 0$.

The expressions for the mean vertical velocities at the surface and bottom boundaries are given by (A19) and (A13), respectively. The mean vertical velocity at $z = 0$, $\langle w_1 (z = 0) \rangle$, is driven by the mean net vorticity transport in the surface Ekman layer, $\langle u_0^T v_{0\xi\xi} \rangle$. The mean vertical velocity at $z = -H$, $\langle w_1 (z = -H) \rangle$, is driven by three mechanisms. The first is Ekman pumping which is proportional to the shelf vorticity $\langle v_{1\xi} \rangle$. The second is $\langle v_0 v_{0\xi} \rangle_\xi$, the net transport of vorticity in the bottom Ekman layer. The third is the interaction of the mean onshore velocity $\langle u_1 \rangle$ with the bottom slope. The mean onshore velocity $\langle u_1 \rangle$ is determined by the gradient of the Reynolds stress $\langle u_0 v_{0\xi} \rangle$ [(3.4)]. Since all terms (except $\langle v_{1\xi} \rangle$) in the vorticity balance (2.10) are determined by the net transport of vorticity and the gradient of a Reynolds stress, $\langle v_{1\xi} \rangle$ is determined by O(1) variables.

The mean alongshore velocity $\langle v_1 \rangle$ may also be explained by mass conservation arguments. The net cross-shelf flow in the interior and Ekman layers driven by the gradients of Reynolds stresses must be balanced by a transport in the bottom Ekman layer. That transport demands the existence of a mean alongshore velocity [Eq. (A12)].

Expressions are derived for $\langle v_1 \rangle$ [(3.12)], the alongshore mean flow, and $\langle u_1 \rangle$ [(3.11)], the cross-shelf mean flow, that depend only on O(1) variables and model parameter values. An expression for $R(u_0, v_{0\xi})$, the cross-correlation coefficient for u_0 and $v_{0\xi}$, that depends only on the topography, friction and forcing frequency was derived in (3.15). This form for $R(u_0, v_{0\xi})$ is independent of the boundary conditions at $\xi = -1$ and ξ_0, and the O(1) variables.

The alongshore mean velocity $\langle v' \rangle$ was found to be independent of δ'_E as $\delta'_E \to 0$ [(5.2)]. For $H(\xi_0) \gtrsim \sqrt{2}\gamma$, the presence of infinitesimal friction is sufficient to generate a finite alongshore mean flow, i.e., $\lim_{\delta'_E \to 0} \langle v' \rangle \neq 0$.

It was shown that the momentum flux and Reynolds stress in the surface and bottom boundary layers contribute to the mean flow. We also determined that for $H(\xi_0) \leq \sqrt{2}\gamma$ the model results are not sensitive to coastal wall height $H(\xi_0)$.

On eastern boundaries the alongshore Eulerian and Lagrangian mean flow, forced by an alongshore wind stress at the coast, has its largest response associated with the first mode resonance and is directed equatorward. The second largest response is associated with the second mode resonance and directed poleward.

The response forced by an imposed oceanic alongshore velocity is a poleward mean velocity with a maximum near the shelf break. The observed eastern boundary undercurrents are poleward and exhibit an offshore maximum.

We conclude that the model results for coastal forcing are inconsistent with the observations of eastern boundary currents, whereas the results for interior forcing are qualitatively consistent with observations.

Acknowledgments. This research was supported by the Oceanography Section of the National Science Foundation under Grants OCE-7826820 and OCE-8026131.

APPENDIX A

Ekman Layer Solutions

We solve for the surface and bottom Ekman layers to obtain the O(1) and O(ϵ) shelf equations in a closed form. The closure is achieved by writing the velocities in the boundary layers as the inviscid interior variables plus a correction and by requiring that (2.3a) and (2.3b) are satisfied. We then have for the Ekman layers,

$$\mathbf{u}(x, y, z, t) = \mathbf{u}^K(x, y, t) + \mathbf{u}^E(x, y, \hat{z}, t), \quad \text{(A1)}$$

where superscript K denotes interior shelf or ocean variables, superscript E denotes surface T ($\hat{z} = \eta = z/\delta_E$) or bottom B [$\hat{z} = \zeta = (z + H)/\delta_E$] Ekman layer variables, and $\mathbf{u}$ is the velocity vector.

Substituting (A1) into (2.1) and subtracting the inviscid interior momentum equation (2.4) yields

$$\delta u_t^E + \tilde{\epsilon}[(u^K + u^E)u_x^E + u^E u_x^K + (v^K + v^E)u_y^E + v^E u_y^K + w^E u_z^E] - v^E = \delta_E{}^2 u_{zz}^E, \quad \text{(A2a)}$$

$$\delta v_t^E + \tilde{\epsilon}[(u^K + u^E)v_x^E + u^E v_x^K + (v^K + v^E)v_y^E + v^E v_y^K + w^E v_z^E] + u^E = \delta_E{}^2 v_{zz}^E, \quad \text{(A2b)}$$

$$u_x^E + v_y^E + w_z^E = 0. \quad \text{(A2c)}$$

The boundary conditions for the Ekman layer equations are obtained by substituting (A1) into (2.3a) and (2.3b) and by requiring the Ekman velocities go to zero away from the boundaries. The resulting boundary conditions for the surface Ekman layer are

$$u_z^T = 0, \quad \delta_E v_z^T = \tau,$$
$$w^T = -w^K(z = 0), \quad \text{at} \quad \eta = 0, \quad \text{(A3a)}$$
$$u^T, v^T, w^T \to 0, \quad \text{as} \quad \eta \to -\infty \quad \text{(A3b)}$$

and for the bottom Ekman layer are

$$u^B = -u^K, \quad v^B = -v^K,$$
$$w^B = -w^K(z = -H), \quad \text{at} \quad \zeta = 0, \quad \text{(A4a)}$$
$$u^B, v^B, w^B \to 0, \quad \text{as} \quad \zeta \to \infty. \quad \text{(A4b)}$$

a. Shelf

The Ekman layer velocities, in the shelf region, are rescaled and expanded in powers of ϵ to yield

$$u^E = \delta^{-1}(u_0^E + \epsilon u_1^E + \cdots), \quad \text{(A5a)}$$
$$v^E = \delta^{-1}(v_0^E + \epsilon v_1^E + \cdots), \quad \text{(A5b)}$$
$$w^B = \delta^{-1}(w_0^B + \epsilon w_1^B + \cdots), \quad \text{(A5c)}$$
$$w^T = \delta^{-1}(w_0^T + \epsilon w_1^T + \cdots). \quad \text{(A5d)}$$

Substituting (A5) and (2.6) into (A2) we obtain the O(1) momentum equations,

$$-v_0^E = u_{0\hat{z}\hat{z}}^E, \quad u_0^E = v_{0\hat{z}\hat{z}}^E. \quad \text{(A6a, b)}$$

For the bottom layer, the depth-integrated mass conservation equation gives

$$w_0(z = -H) = -\delta_E \delta^{-1} \int_0^\infty u_{0\xi}^B d\zeta - H_\xi u_0, \quad \text{(A7)}$$

where (A4) has been utilized. At O(ϵ) the time averaged momentum equations are

$$-\langle v_1^B \rangle = \langle u_1^B \rangle_{\zeta\zeta} - \left\langle u_0^B u_{0\xi}^B - u_{0\zeta}^B \int_0^\zeta u_{0\xi}^B d\zeta' \right\rangle, \quad \text{(A8a)}$$

$$\langle u_1^B \rangle = \langle v_1^B \rangle_{\zeta\zeta} - \left\langle u_0^B v_{0\xi}^B + u_0^B v_{0\xi} - v_{0\zeta}^B \int_0^\zeta u_{0\xi}^B d\zeta' \right\rangle, \quad \text{(A8b)}$$

and the depth-integrated time-averaged mass conservation equation is

$$\langle w_1(z = -H) \rangle = -\delta_E \delta^{-1} \int_0^\infty \langle u_{1\xi}^B \rangle d\zeta - H_\xi \langle u_1 \rangle. \quad \text{(A9)}$$

From the standard solutions to (A6) with boundary conditions obtained from (A4) it follows that,

$$\int_0^\infty u_0^B d\zeta = -v_0/\sqrt{2}, \quad \text{(A10)}$$

$$w_0(z = -H) = \gamma v_{0\xi} - H_\xi u_0, \quad \text{(A11)}$$

where $\gamma = \delta_E(\delta\sqrt{2})^{-1}$ [(2.16b)]. The solution to (A8) with the boundary conditions obtained from (A4) may be readily obtained and the results corresponding to (A10) and (A11) are

$$\int_0^\infty \langle u_1^B \rangle d\zeta = -\langle v_1 \rangle/\sqrt{2} + (7/20)/\sqrt{2}\langle v_0 v_{0\xi} \rangle \quad \text{(A12)}$$

and

$$\langle w_1(z = -H) \rangle = -\gamma[-\langle v_1 \rangle_\xi + (7/20)\langle v_0 v_{0\xi} \rangle_\xi] - H_\xi \langle u_1 \rangle. \quad \text{(A13)}$$

For the surface Ekman layer,

$$w_{0\eta}^T = 0 \quad \text{(A14)}$$

and

$$-\langle v_1^T \rangle = \langle u_{1\eta\eta}^T \rangle, \quad \text{(A15a)}$$
$$\langle u_1^T \rangle = \langle v_{1\eta\eta}^T \rangle - \langle u_0^T v_{0\xi} \rangle, \quad \text{(A15b)}$$
$$\langle w_{1\eta}^T \rangle = -\sqrt{2}\gamma \langle u_{1\xi}^T \rangle. \quad \text{(A15c)}$$

From the solutions to (A6) and (A15) with boundary conditions derived from (A3) it follows that

$$\int_{-\infty}^{0} u_0^T d\eta = \tau, \tag{A16}$$

$$w_0\,(z = 0) = 0, \tag{A17}$$

and

$$\int_{-\infty}^{0} \langle u_1^T \rangle d\eta = -\langle \tau v_{0\xi} \rangle, \tag{A18}$$

$$\langle w_1\,(z = 0) \rangle = -\sqrt{2}\gamma \langle \tau v_{0\xi\xi} \rangle. \tag{A19}$$

b. Interior ocean

The solutions to the Ekman layers in the interior ocean may be formed in a similar manner. The results for both the bottom and surface Ekman layers are at O(1),

$$w_0^I\,(z = -H) = (v_{0x}^I - u_{0y}^I)/\sqrt{2}, \tag{A20a}$$

$$w_0^I\,(z = 0) = \tau_x, \tag{A20b}$$

and at O(ϵ),

$$\langle w_1^I\,(z = -H) \rangle = \langle v_{1x}^I \rangle/\sqrt{2}, \tag{A21a}$$

$$\langle w_1^I\,(z = 0) \rangle = 0. \tag{A21b}$$

APPENDIX B

O(1) Numerical Solution

A solution to (3.1) in the form (3.3) is facilitated by writing (3.1) as four coupled first-order ordinary differential equations for the four real variables $Y^{(i)}$, $i = 1, 4$:

$$Y_\xi^{(1)} = Y^{(2)}, \tag{B1a}$$

$$Y_\xi^{(2)} = -H_\xi K[\gamma(\omega Y^{(4)} - lY^{(3)}) + \omega H(\omega Y^{(2)} - lY^{(1)})], \tag{B1b}$$

$$Y_\xi^{(3)} = Y^{(4)}, \tag{B1c}$$

$$Y_\xi^{(4)} = H_\xi K[\gamma(\omega Y^{(2)} - lY^{(1)}) - \omega H(\omega Y^{(4)} - lY^{(3)})], \tag{B1d}$$

where $\psi = Y^{(1)} + iY^{(3)}$ and $K = [(\omega H)^2 + \gamma^2]^{-1}$.

Utilizing (3.3) with (3.2) and (2.20), we find the boundary conditions,

$$Y^{(2)} = \sqrt{2}\sin\phi - H\gamma^{-1}(\omega Y^{(4)} - lY^{(3)}), \quad \text{at} \quad \xi = 0, \tag{B2a}$$

$$Y^{(4)} = H\gamma^{-1}(\omega Y^{(2)} - lY^{(1)}), \quad \text{at} \quad \xi = 0, \tag{B2b}$$

$$Y^{(2)} = \gamma J, \quad Y^{(4)} = \omega J, \quad \text{at} \quad \xi = -1, \tag{B3a, b}$$

where $J = \sqrt{2}k\gamma(k\sin\phi + l\cos\phi)[(k^2 + l^2)(\omega^2 + \gamma^2)]^{-1}$.

We solve (B1), with the boundary conditions (B2) and (B3), using a fifth-order Runge-Kutta method. Four independent *initial-value* problems are created by rewriting the boundary conditions such that only one inhomogeneous condition is specified for each initial-value problem (Acton, 1970). For example, using a subscript on Y to denote the respective initial-value problem, the boundary condition for these problems, from (B2) and (B3), are

$$Y_1^{(1)} = 1, \quad Y_1^{(2)} = \gamma J, \quad Y_1^{(3)} = 0, \quad Y_1^{(4)} = 0, \quad \text{at} \quad \xi = -1, \tag{B4}$$

$$Y_2^{(1)} = 0, \quad Y_2^{(2)} = 0, \quad Y_2^{(3)} = 1, \quad Y_2^{(4)} = \omega J, \quad \text{at} \quad \xi = -1, \tag{B5}$$

$$\left.\begin{aligned} Y_3^{(1)} = 0,\ Y_3^{(2)} = \sqrt{2}\sin\phi - H\gamma^{-1}(\omega - l) \\ Y_3^{(3)} = 1,\ Y_3^{(4)} = 1 \end{aligned}\right\} \text{at } \xi = 0, \tag{B6}$$

$$\left.\begin{aligned} Y_4^{(1)} = 1, \quad Y_4^{(2)} = 1 \\ Y_4^{(3)} = 0, \quad Y_4^{(4)} = H\gamma^{-1}(\omega - l) \end{aligned}\right\} \text{at} \quad \xi = 0. \tag{B7}$$

The four independent linear solutions are then superimposed to give the solution to the boundary value problem, i.e.,

$$Y^{(i)} = \sum_{j=1}^{4} B_j Y_j^{(i)}, \quad \text{for} \quad i = 1, 4. \tag{B8}$$

A system of four linear, homogeneous equations in the four unknowns, $B_1, \ldots, B_4$, may be found from the requirement that $Y^{(i)}$ satisfy the boundary conditions (B2) and (B3). Solving for $B_1, \ldots, B_4$, we then have the solution to the boundary value problem directly without using an iterative technique. The method was tested by comparing the numerical solutions with analytical solutions obtainable in the small slope limit, $H_\xi \ll 1$.

APPENDIX C

O(1) Free-Wave Solution

Equations governing the free-wave solution to (3.1), with boundary conditions (2.20) and (3.2), are found by setting the forcing equal to zero, i.e. $\phi = k = 0$. The result is an eigenvalue problem. A wave-like solution of the form

$$p_0 = \mathrm{Re}\{\psi(\xi)\exp[i(ly - (\alpha - i\beta)t)]\} \tag{C1}$$

is used, where $\psi(\xi)$ is the complex eigenfunction and $(\alpha - i\beta)$ is the complex eigenvalue (α, β real). We determine ψ, β and α with a shooting method, that is, for each l we adjust γ and α until the boundary conditions are satisfied.

A summary of the results, using the parameter values given in Table 1, are presented in Table 2. The

TABLE 2. Free wave mode characteristics.

Mode	ω'/f	β'/f	$2\pi/\omega'$ (days)	β'^{-1} (days)	ω'/l' (km day^{-1})
1	0.246	0.0142	3.0	8.2	333
2	0.061	0.0197	11.9	5.9	84
3	0.025	0.0086	29.1	13.5	34

presence of friction in the model causes the long, free waves to be dispersive (Fig. 10). The *e*-folding time varies with frequency and wavenumber (Fig. 10). The phase speeds and periods for modes 1 and 2 calculated with the depth profile used here are consistent with those obtained from calculations for Oregon by Cutchin and Smith (1973). The decay time scale generally is longer than the period for the first mode and shorter than the period for higher modes.

Allen and Smith (1981) examined data from the Oregon shelf (45°16′N; see Fig. 2) taken during July and August 1973 at a mid-shelf location (100 m depth). Terms in the depth-integrated alongshore momentum balance were estimated, including a calculation of the bottom stress using the quadratic drag law on hourly data ($C_D = 1.5 \times 10^{-3}$). They showed that for low-pass filtered (40 h half-power point) data the linear approximation $\tau_B = rv_B$, where subscript B denotes values near the bottom, was reasonably good and by a regression of τ_B on v_B obtained an estimate of $r = 2 \times 10^{-2}$ cm s^{-1}. The equivalent "resistance" coefficient used here, $fH_0\delta_E/\sqrt{2} = 2.8 \times 10^{-2}$ cm s^{-1}, is close to that value.

A spindown time of 6.8 days was also estimated by Allen and Smith. This compares with the first and second mode spindown times here of 8.2 and 5.9 days. Peaks in the spectra of depth integrated v_t were found at 0.1 and 0.34 cycle per day. If these peaks correspond to a resonant response, we note that the corresponding wavelengths for these frequencies for mode 1 are 1100 and 300 km and for mode 2 are 500 and 1300 km, respectively. The wavelength used here is 1000 km.

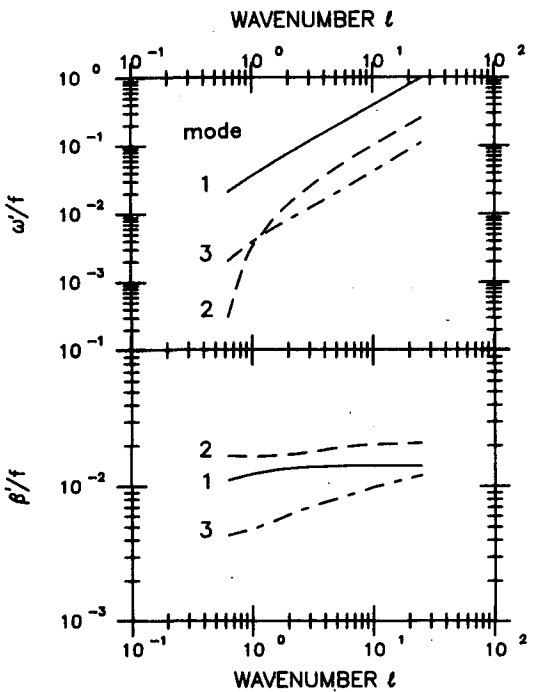

FIG. 10. Free-wave dispersion curves for modes 1–3. Parameter values used are listed in Table 1. The dispersion curve plotted as a function of ω'/f and l and as a function of β'/f and l are displayed in the top and bottom rows, respectively.

APPENDIX D

Parameter Values

The parameter values used in this paper (Table 1) are based on the conditions thought to be typical for the Oregon continental margin (see Appendix C).

The model dependence on ω, the forcing frequency, is explored by varying ω' from $0.02f$ to $0.32f$. Variations in the parameters listed in Table 1 are found to have little qualitative effect on the results. The magnitude of the response is sensitive to the values chosen for f, δ_E' and τ_0.

REFERENCES

Acton, F. S., 1970: *Numerical Methods that Work.* Harper and Row, p. 158.

Allen, J. S., 1976: On forced, long continental shelf waves on an *f*-plane. *J. Phys. Oceanogr.*, **6**, 426–431.

——, and R. L. Smith, 1981: On the dynamics of wind-driven shelf currents. *Phil. Trans. Roy. Soc. London*, **A302**, 617–634.

Brink, K. H., and J. S. Allen, 1978: On the effect of bottom friction on barotropic motion over the continental shelf. *J. Phys. Oceanogr.*, **8**, 919–922.

Brockmann, C., E. Fahrbach, A. Huyer and R. L. Smith, 1980: The poleward undercurrent along the Peru coast: 5 to 15°S. *Deep-Sea Res.*, **27A**, 847–856.

Caldwell, D. R., and S. A. Eide, 1976: Experiments on the resonance of long period waves near islands. *Proc. Roy. Soc. London*, **A348**, 359–378.

Colin de Verdière, A., 1979: Mean flow generation by topographic Rossby waves. *J. Fluid Mech.*, **94**, 39–64.

Cutchin, D. L., and R. L. Smith, 1973: Continental shelf waves: Low-frequency variations in sea level and currents over the Oregon continental shelf. *J. Phys. Oceanogr.*, **3**, 73–82.

Halpern, D., R. L. Smith and R. K. Reed, 1978: On the California Undercurrent over the continental slope off Oregon. *J. Geophys. Res.*, **83**, 1366–1372.

Hickey, B. M., 1979: The California Current System—hypothesis and facts. *Prog. Oceanogr.*, **8**, 191–279.

——, 1982: The California Undercurrent and adjacent shelf currents during summer, 1972. Submitted to *J. Mar. Res.*

Huthnance, J. M., 1973: Tidal current asymmetries over the Norfolk Sandbanks. *Estuarine Coast. Mar. Sci.*, **1**, 89–99.

——, 1981: On mass transports generated by tides and long waves. *J. Fluid Mech.*, **102**, 367–387.

Loder, J. W., 1980: Topographic rectification of tidal currents on the sides of Georges Bank. *J. Phys. Oceanogr.*, **10**, 1399–1416.

Longuet-Higgins, M. S., 1969: On the transport of mass by time-varying ocean currents. *Deep-Sea Res.*, **16**, 431–447.

McEwan, A. D., R. O. R. Y. Thompson and R. A. Plumb, 1980: Mean flows driven by weak eddies in rotating systems. *J. Fluid Mech.*, **99**, 655–672.

Peffley, M. B., and J. J. O'Brien, 1976: A three-dimensional simulation of coastal upwelling off Oregon. *J. Phys. Oceanogr.*, **6**, 164–180.

Spillane, M. C., 1980: A model of wind-forced viscous circulation near coastal boundaries. Ph.D. thesis, Oregon State University.

Wooster, W. S., and J. L. Reid, 1963: Eastern boundary currents. *The Sea*, Vol. 2, M. N. Hill, Ed., Wiley, 253–280.